Phase space entropies and global quantum phase space organisation: A two-dimensional anharmonic system

G Groh†, H J Korsch† and W Schweizer‡§

† FB Physik, Universität Kaiserslautern, D-67653 Kaiserslautern, Germany
‡ Institut for Astronomie und Astrophysik, Abteilung Theoretische Astrophysik, Universität Tübingen, Auf der Morgenstelle 10, D-72076 Tübingen, Germany

Abstract. The global dynamical properties of a quantum system can be conveniently visualized in phase space by means of a quantum phase space entropy in analogy to a Poincaré section in classical dynamics for two-dimensional time independent systems. Numerical results for the Pullen–Edmonds systems demonstrate the properties of the method for systems with mixed chaotic and regular dynamics.

PACS numbers: 03.65.-w, 05.45.+b

Submitted to: *J. Phys. A: Math. Gen.*

1. Introduction

Recently, it has been demonstrated for the case of one-dimensional time-periodic systems that the global quantum dynamics of a system can be conveniently analysed and visualized by means of a quantum phase space entropy [1, 2, 3]. In close analogy to the celebrated Poincaré surface of section in classical dynamics, which visualizes the global dynamical properties by a synoptic portray of trajectories in phase space by means of their consecutive intersections with a plane, the quantum dynamics can be visualized by means of the time-averaged localization of wave packets on such a plane. A more general discussion of the properties of these quantum phase space entropies can be found in [4].

In the present paper, we extend the previous studies of time-periodically driven systems with a single degree of freedom, where a stroboscopic plot of the phase space points at integer multiples of the driving period has been used, to the more demanding case of Hamiltonian systems with two degrees of freedom

$$H = \frac{1}{2}\left({p_x}^2 + {p_y}^2\right) + V(q_x, q_y)\,. \tag{1}$$

§ Present address: Theoretische Physik I, Fakultät für Physik und Astronomie, Ruhr-Universität Bochum, D-44780 Bochum, Germany

As an illustrating expample, we will discuss the Pullen–Edmonds [5] system

$$V(q_x, q_y) = \frac{1}{2}\left(q_x^2 + q_y^2\right) + \alpha\, q_x^2 q_y^2\,, \tag{2}$$

which has been used by various authors to study the classical/quantum correspondence for classically chaotic systems [5]–[10]. By scaling the variables, it can be shown that the classical dynamics depends only on the product of the nonlinearity parameter α and the energy E . It is therefore sufficient to fix the energy at, e.g., $E = 20$ and vary the parameter α. Figure 1 shows Poincaré sections

$$q_y = 0 \qquad \text{and} \qquad p_y = p_y^{(E)} = +\left(2(E - V(q_x, 0)) - p_x^2\right)^{1/2}\,, \tag{3}$$

at $E = 20$ for $\alpha = 0.025$, 0.05, 0.075, and 0.1 . Note that the centre, $(p_x, q_x) = (0, 0)$, the kinetic energy in the y-direction has its maximum value, i.e. $p_y = (2E)^{1/2}$, whereas we have $p_y = 0$ at the outer outer circle $p_x^2 + q_x^2 = 2E$. Note also that the region outside this circle is not empty because of *dynamical* restrictions, but only because of *geometrical* reasons: there is no intersection of the energy shell $H(\vec{p}, \vec{q}) = E$ with the subspace $q_y = 0$.

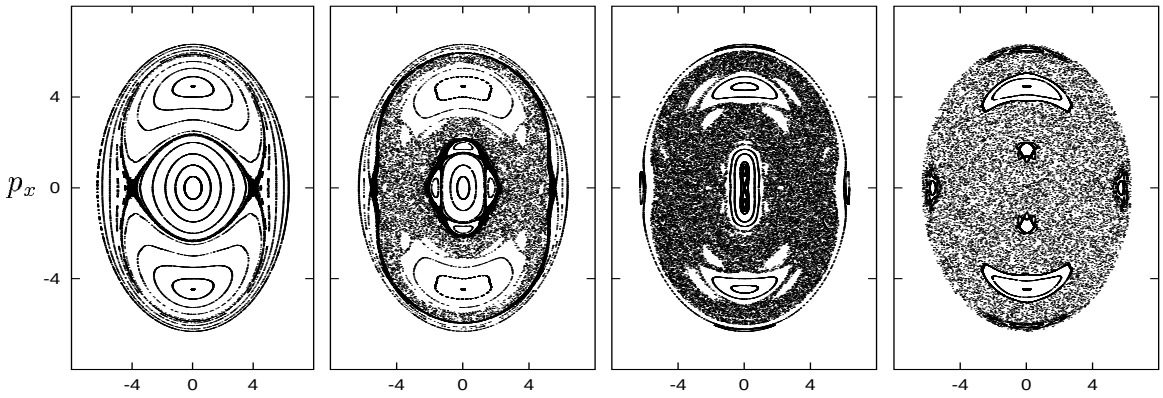

Figure 1. Classical Poincaré sections for the Pullen–Edmonds system (2) for an energy $E = 20.0$ and increasing nonlinearity parameter $\alpha = 0.025$, 0.05, 0.075, 0.1.

For small α the dynamics is predominantly regular. There is a pair of stable periodic orbits along the q_x and the q_y axis, which appear as a central stability island at $(p_x, q_x) = (0, 0)$ or as a full circle $p_x^2 + q_x^2 = 2E = 40$, e.g. the outer boundary) in the Poincaré plot in figure 1, respectively. For the future discussion we note that the inner and outer regions of the Poincaré section are directly related by the symmetry $q_x \leftrightarrow q_y$. In addition, there are two periodic orbits along the diagonals $q_y = \pm q_x$, which show up as stability islands at $(p_x, q_x) = (\pm(E)^{1/2}, 0) \approx (\pm 4.5, 0)$. The anharmonic perturbation breaks the coordinate – momentum symmetry of the harmonic oscillator and the corresponding momentum space trajectories $p_y = \pm p_x$ (circles in coordinate space with radius $\approx (E)^{1/2} \approx 4.5$) are unstable and appear as hyperbolic fixed points in figure 1 at $(p_x, q_x) \approx (0, 4.5)$. Chaotic motion first shows up in the vicinity of these points.

With increasing α, the chaotic region grows and more elliptic/hyperbolic island chains appear, as, e.g., the chain of four satellite islands of the central island for $\alpha = 0.05$ (by symmetry, these islands are also observable close to the outer boundary) and a further increase of α leads to a bifurcation of the central fixed point ($\alpha = 0.075$) followed by a loss of stability and a further growth of the chaotic 'sea' between the islands. For $\alpha = 0.1$ only a few regular regions are observed in figure 1: Four islands close to the boundary centred at $(p_x, q_x) \approx (\pm 6, 0)$ or $(0, \pm 6)$; two larger resonances at $(\pm 4.5, 0)$ and two smaller ones at $(\pm 1.7, 0)$ (note that the last two are related to the four outer ones by the exchange symmetry $q_x \leftrightarrow q_y$). We will show, that this characteristic classical scenario is also observable in quantum mechanics.

In the following section, we give a brief outline of the Husimi phase space distribution for eigenstates of the Pullen–Edmonds Hamiltonian (2) and demonstrate that the classical dynamical properties are reflected in some of the *individual* quantum states. In addition, the localization of the quantum states on the energy shell (3) is discussed. The *global*, i.e. state independent, phase space properties of the quantum system are analysed in Sect. 3. We summarize our results in Sect. 4.

2. Phase space densities of individual states

The symmetry group of the Pullen–Edmonds Hamiltonian (2) is C_{4v} and the eigenstates can be classified by the four one dimensional irreducible representations $\mathcal{A}_1, \mathcal{A}_2, \mathcal{B}_1, \mathcal{B}_2$ and the two dimensional representation $\mathcal{E}$ [5]. Within each symmetry group $\mathcal{S}$, the eigenstates are expanded in terms of symmetry adapted harmonic oscillator wave functions $|\phi_j^{\mathcal{S}}\rangle$, i.e. eigenstates of the Hamiltonian for $\alpha = 0$, which are given by $|n_x^e\rangle \otimes |n_y^e\rangle + |n_y^e\rangle \otimes |n_x^e\rangle$ for class $\mathcal{A}_1$, by $|n_x^o\rangle \otimes |n_y^o\rangle - |n_y^o\rangle \otimes |n_x^o\rangle$ for $\mathcal{A}_2$, by $|n_x^e\rangle \otimes |n_y^e\rangle - |n_y^e\rangle \otimes |n_x^e\rangle$ for $\mathcal{B}_1$, and by $|n_x^o\rangle \otimes |n_y^o\rangle + |n_y^o\rangle \otimes |n_x^o\rangle$ for $\mathcal{B}_2$, where even and odd states are denoted by e or o, respectively. In addition, these states are multiplied by the normalisation factor $(2(1 + \delta_{n_1 n_2}))^{-1/2}$. In this basis, the matrix elements of the Hamiltonian (2) can be easily evaluated analytically (a band matrix) and the eigenvalues E_ν and eigenvectors $|\psi_\nu\rangle = \sum_j c_j^{(\nu)} |\phi_j^{\mathcal{S}}\rangle$ are computed by means of the spectral transformation method of Lanczos [11]. The (degenerate) states of class $\mathcal{E}$ are not explicitly considered here (the interested reader can find a discussion of the computation and the properties of these states in [12]).

Classically, an estimate of the number of quantum states $N^{\mathrm{cl}}(E)$ up to an energy E is given by the Weyl rule:

$$N^{\mathrm{cl}}(E) = \int \frac{\mathrm{d}\vec{p}\,\mathrm{d}\vec{q}}{(2\pi\hbar)^f}\, \theta(E - H(\vec{p}, \vec{q})) \tag{4}$$

in excellent agreement with the quantum staircase function

$$N(E) = \sum_{\nu=1}^{\infty} \theta(E - E_\nu) = \mathrm{Tr}\, \theta(E - \hat{H})\,. \tag{5}$$

Expanding the integrand in powers of the coupling constant α, a useful approximation

$$N^{\rm cl}(E,\alpha) \approx \frac{E^2}{2\hbar^2}\,\left(1-\frac{\alpha}{3}E\right) \tag{6}$$

can be derived. In the present analysis, we have computed 5500 states up to an energy of $E \approx 30$. In addition, we note that the density of states is high, e.g. $\mathrm{d}N/\mathrm{d}E \approx 230$ for $E = 20$.

As demonstrated in various studies before, not only the number of eigenstates, but also the individual eigenstates themselves are intimately linked to the classical phase space structure shown in figure 1. However, the *individual* states are more or less supported by the various classical phase space structures, which can be conveniently shown by inspecting the morphology of quantum (Husimi) phase space densities.

2.1. Individual Husimi phase space distributions

The Husimi distribution of a quantum wavefunction $|\psi\rangle$ is given by

$$\rho^{\rm H}(\vec{p},\vec{q}) = |\langle\vec{\alpha}|\psi\rangle|^2 \ , \tag{7}$$

where $|\vec{\alpha}\rangle = |\alpha_x\rangle|\alpha_y\rangle$ is a two-dimensional coherent oscillator state, i.e.

$$|\alpha\rangle = \mathrm{e}^{-|\alpha|^2/2}\,\sum_{n=0}^{\infty}\,\frac{\alpha^n}{n!}\,(\hat{a}^\dagger)^n|0\rangle = \mathrm{e}^{-|\alpha|^2/2}\,\sum_{n=0}^{\infty}\,\frac{\alpha^n}{\sqrt{n!}}\,|n\rangle \ . \tag{8}$$

in the harmonic oscillator basis $|n\rangle$. The complex variable α can be mapped onto phase space by $\alpha = (q+\mathrm{i}p)/\sqrt{2\hbar}$, and the coherent states can also be labelled as $|\vec{\alpha}\rangle = |\vec{p},\vec{q}\rangle$, i.e. by the phase space point where the Gaussian distribution of the coherent state is localized. The Husimi distribution of a harmonic oscillator state is

$$\rho^{\rm H}_n(p,q) = \,|\,\langle\alpha|n\rangle\,|^2 = \left|\,\mathrm{e}^{-\frac{|\alpha^*|^2}{2}}\,\frac{(\alpha^*)^n}{\sqrt{n\,!}}\,\right|^2 = \left|\,\mathrm{e}^{-\frac{I}{4\hbar}}\,\left(\frac{I}{2\hbar}\right)^{\frac{n}{2}}\mathrm{e}^{-\mathrm{i}n\theta}\frac{1}{\sqrt{n\,!}}\,\right|^2 \tag{9}$$

with $I = q^2+p^2$ and θ is the polar angle in the (p,q) plane. For a linear combination of oscillator states one simply gets a a linear combination of these terms and for the present case of the coupled two dimensional oscillator (2) one has

$$\begin{aligned}\rho^{\rm H}_\nu(p_x,p_y,q_x,q_y) &= |\langle\vec{\alpha}|\psi_\nu\rangle|^2 \\ &= \mathrm{e}^{-\frac{I_x+I_y}{2\hbar}}\sum_{n_1,n_2}{}'\sum_{n_1',n_2'}{}' C^{(\nu)}_{n_1n_2}\,C^{(\nu)}_{n_1'n_2'}\,\left(\frac{I_x}{2\hbar}\right)^{\frac{n_1}{2}}\left(\frac{I_y}{2\hbar}\right)^{\frac{n_2}{2}}\left(\frac{I_x}{2\hbar}\right)^{\frac{n_1'}{2}}\left(\frac{I_y}{2\hbar}\right)^{\frac{n_2'}{2}}\times \\ &\times\,\frac{1}{\sqrt{n_1!\,n_2!\,n_1'!\,n_2'!}}\,\cos\left((n_1-n_1')\,\theta_x+(n_2-n_2')\,\theta_y\right) \ ,\end{aligned} \tag{10}$$

with $I_x = q_x^2+p_x^2, \ldots$. The $C^{(\nu)}_{n_1n_2}$ are computed expansion coefficients of the eigenstates in the oscillator basis and the primed sum denotes a summation over the symmetry selected basis states, i.e. $n_1 = 0,2,2,4,6,\ldots$ and $n_2 = 0,0,2,2,0,\ldots$ for class $\mathcal{H}_{\mathcal{A}_1}$. This circumvents a numerical evaluation of the oscillatory integrals for the computation of the Husimi distributions.

The Husimi distributions $\rho_\nu^{\mathrm{H}} = |\langle\vec{\alpha}|\psi_\nu\rangle|^2$ of individual eigenstates of the Hamiltonian (1) with eigenvalue E_ν have been considered by many authors to investigate the classical quantum correspondence by comparison of $\rho_\nu^{\mathrm{H}}(p_x, p_y^{(E)}, q_x, 0)$ with the classical Poincaré section (3) at an energy $E = E_\nu$ (see, e.g., [8, 13]–[16])). The quantum states can be distinguished by means of the localization on the classical phase space structures (e.g. chaotic regions, regular islands surrounded by invariant curves, localization by cantori).

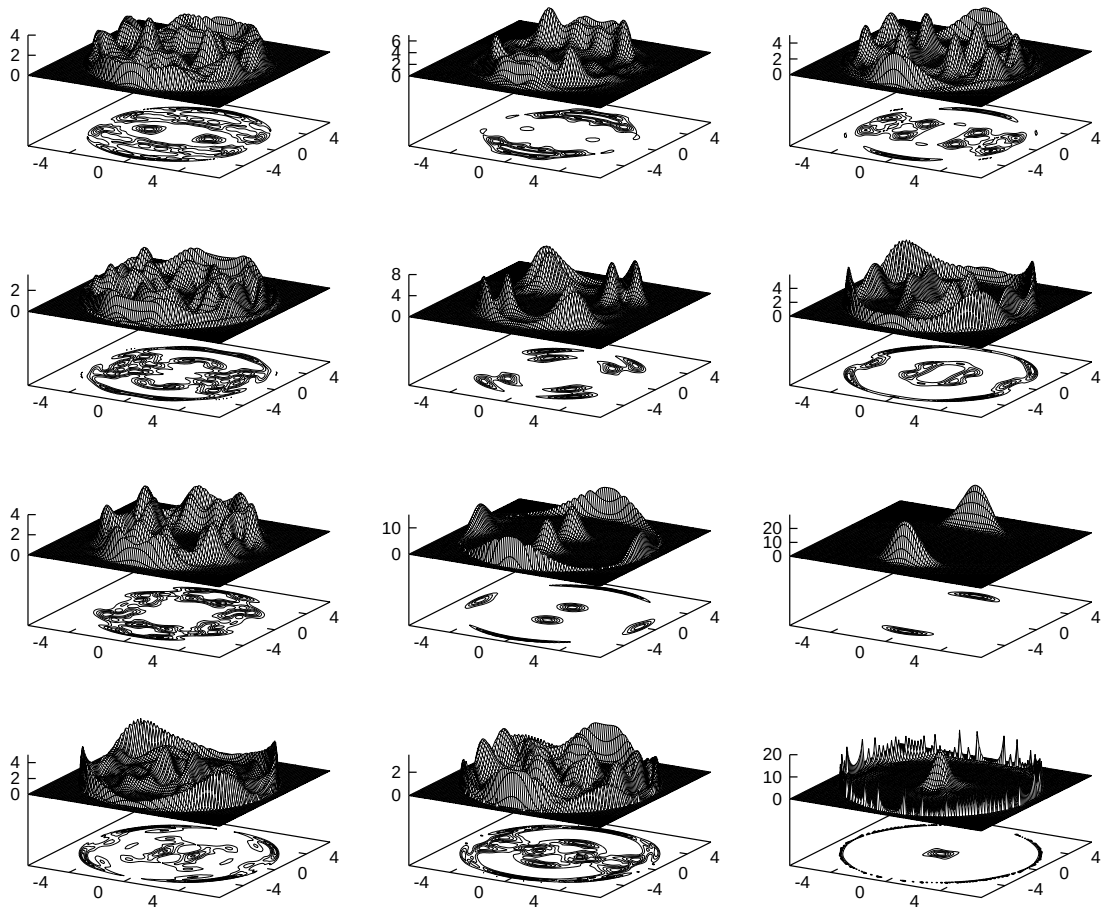

Figure 2. Quantum (Husimi) phase space densities on the (q_x, p_x)–plane for the Pullen–Edmonds system ($\alpha = 0.1$, $\hbar = 0.25$).

A few examples of Husimi distributions for twelve selected states with energies close to $E_\nu \approx 20$ are shown in figure 2 ($\alpha = 0.1$). The states are ordered from the upper left to the lower right one with increasing energies $E_\nu = 20.030$, 20.041, 20.116, 20.175, 20.070, 20.313, 20.136, 20.379, 20.262, 20.248, 20.331, 20.378 and we will number them by (1), (2),.... States (1,2,6,9,10) belong to symmetry class $\mathcal{A}_1$, state (8) to class $\mathcal{A}_2$, (5,7,11,12) to class $\mathcal{B}_1$, state (4) to $\mathcal{B}_2$ and state (3) to class $\mathcal{E}$.

State (9) clearly localizes on the pair of large stability islands centred at $(P_x, q_x) \approx (\pm 4.5, 0)$ in the classical Poincaré section (figure 1). State (8) localizes on the two islands

at $(\pm 1.7, 0)$ and the four islands close to the boundary centred at $(p_x, q_x) \approx (\pm 6, 0)$ or $(0, \pm 6)$, which are related by the symmetry $q_x \leftrightarrow q_y$. It is well known that quantum states can also localize on unstable periodic orbits, as for example the state (12), which strongly populates the central hyperbolic fixed point and, of course, because of symmetry the outer boundary of the Poincaré section. Similarly, state (5) localizes on the already destroyed chain of four satellite island, which are still visible in the classical Poincaré sections (figure 1) for $\alpha = 0.075$. Some other states can be described as "excited" states of the ones described above, as, e.g., states (2) and (6), which appear as excited versions of states (9) and (12), respectively. The other states shown localize more or less on the classically chaotic region.

2.2. Localization on the energy shell

Intuitively, we expect that an eigenstate $|\psi_\nu\rangle$ with energy E_ν is localized on the (classical) energy surface $H(\vec{p}, \vec{q}) = E_\nu$. This can be, however, only approximately true, because such a state populates also phase space regions at energies $E \neq E_\nu$. The localization of individual eigenstates $|\psi_\nu\rangle$ with eigenenergy E_ν on the energy shell $H(\vec{p}, \vec{q}) = E$ can be quantitatively described by the integral of the Husimi density over this energy shell

$$A_\nu(E) = \int\limits_{\mathrm{PSOS}} \frac{\mathrm{d}p_x \mathrm{d}q_x}{2\pi\hbar} \; |\langle \vec{\alpha} | \psi_\nu \rangle|^2 = \int\limits_{p_y^2 \leq 2E} \frac{\mathrm{d}p_x \mathrm{d}q_x}{2\pi\hbar} \; \rho_\nu^{\mathrm{H}} \left(p_x, p_y^{(E)}, q_x, 0 \right) . \qquad (11)$$

It is instructive to analyse first the simple case of eigenstates $|\psi_{n_1 n_2}\rangle = |n_1\rangle \otimes |n_2\rangle$ of a two-dimensional harmonic oscillator with energy $E_{n_1 n_2} = \hbar(n_1 + n_2 + 1)$. Using (9), the Husimi density is

$$\rho^{\mathrm{H}}_{n_1 n_2}(\vec{p}, \vec{q}) = |\langle \vec{\alpha} | \psi_{n_1 n_2} \rangle|^2 = \exp\left(-\frac{I_x + I_y}{2\hbar} \right) \frac{1}{n_1!\, n_2!} \left(\frac{I_x}{2\hbar} \right)^{n_1} \left(\frac{I_y}{2\hbar} \right)^{n_2} . \qquad (12)$$

On the Poincaré section (3) we have $I_y = 2E - I_x$ and therefore

$$A_{n_1 n_2}(E) = \frac{1}{4\pi\hbar} \int\limits_0^{2E} \mathrm{d}I \int\limits_0^{2\pi} \mathrm{d}\theta \; \mathrm{e}^{-E/\hbar} \; \frac{1}{n_1!\, n_2!} \left(\frac{I}{2\hbar} \right)^{n_1} \left(\frac{2E - I}{2\hbar} \right)^{n_2} . \qquad (13)$$

With $\int\limits_0^1 \mathrm{d}u \; u^n \, (1-u)^m = n!\, m!/(n+m+1)!$ we obtain

$$A_{n_1 n_2}(E) = \frac{1}{(n_1 + n_2 + 1)!} \, \mathrm{e}^{-E/\hbar} \left(\frac{E}{\hbar} \right)^{n_1 + n_2 + 1} \qquad (14)$$

or by normalising to unit integral over the energy E the function $\widetilde{A}_{n_1 n_2}(E) = A_{n_1 n_2}(E)/\hbar$ of a given eigenstate, which is a Gamma distribution in E with a maximum at $E_{\max} = E_{n_1 n_2}$, average value $\langle E \rangle = E_{n_1 n_2} + \hbar$ and variance $(\Delta E)^2 = \hbar^2 (E_{n_1 n_2}/\hbar + 1)$.

Note that this distribution can also be read as a probability distribution of the eigenstates $(n_1\, n_2)$ on an energy shell with fixed energy E. Completeness of the eigenstates immediately yields

$$\sum_{n_1 n_2} A_{n_1 n_2}(E) = \int\limits_{p_y^2 \leq 2E} \frac{\mathrm{d}p_x \mathrm{d}q_x}{2\pi\hbar} = \frac{E}{\hbar} \qquad (15)$$

and the renormalized distribution of the eigenstates on the energy shell is Poisson distributed with a maximum at $E_{n_1 n_2\,(\max)} \approx E + \hbar/2 - \hbar^2/(24E)$, average value $\langle E_{n_1 n_2} \rangle = E + \hbar$ and variance $(\Delta E_{n_1 n_2})^2 = \hbar E$.

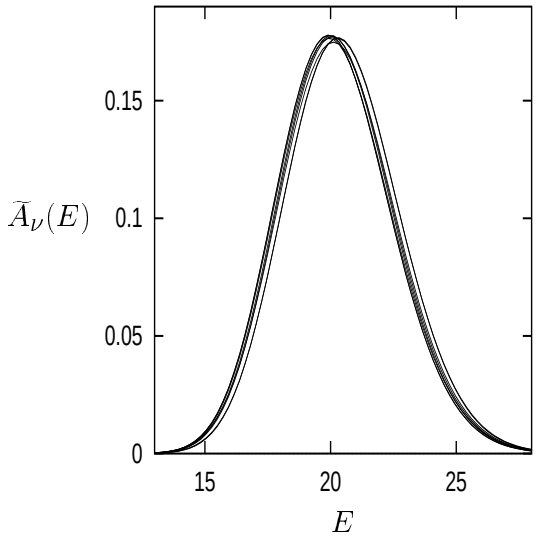

Figure 3. The density on the energy shell $\widetilde{A}_\nu(E)$ (normalized to unity when integrated over E) as a function of the Poincaré section energy E for the Pullen–Edmonds system for eight states with $\alpha = 0.025,\ 0.05,\ 0.075,\ 0.1$, and $\hbar = 0.25,\ 0.75$ and $E_\nu \approx 20$ belonging to different symmetry classes.

Therefore, we can assume that – up to a normalisation factor – the localization of the eigenstates with energy E_ν on a Poincaré section at energy E is Poissonian distributed according to

$$A_\nu(E) \sim \frac{\mathrm{e}^{-E/\hbar}}{\Gamma(E_\nu/\hbar + 1)} \left(\frac{E}{\hbar}\right)^{E_\nu/\hbar} . \tag{16}$$

This is exactly true for the harmonic oscillator. For the Pullen–Edmonds system (2) , figure 3 shows the numerically computed distribution $\widetilde{A}_\nu(E)$ for eight states with $\alpha = 0.025,\ 0.05,\ 0.075,\ 0.1$, and $\hbar = 0.25,\ 0.75$ and $E_\nu \approx 20$ belonging to different symmetry classes as a function of the Poincaré section energy E. All curves almost coincide and are surprisingly well described by the Poisson distribution (16), despite of the fact that the states show different individual phase space localization structures (compare figure 2). Even more surprising is the insensitivity of the E_ν dependence with respect to a non-harmonic term in the Hamiltonian, as illustrated in figure 4 for a Poincaré section energy $E = 20$ and $\alpha = 0.1$, $\hbar = 0.25$. Shown are states of symmetry class $\mathcal{A}_1$ (similar results were found for the other symmetry classes). The overall dependence is well described by (16). The observed differences appear for states which localize strongly at the boundary and at the centre of the classical Poincaré section, which have smaller values of $\widetilde{A}$ (compare the last subplot of figure 2; similar anomalous features of such 'sombrero' states have been reported previously [6]). As for

the case of the two dimensional harmonic oscillator, the distributions have a maximum at $E_{\nu\,(\max)} \approx E + \hbar/2 - \hbar^2/(24E) = 20.125$, mean value $\langle E_\nu \rangle \approx E + \hbar = 20.25$ and variance $(\Delta E_\nu)^2 = \hbar E = 5$ for $E = 20$ and $\hbar = 0.25$. The number of states contributing significantly to the energy shell E, i.e. those in an interval $E \pm \Delta E_\nu$, can therefore be estimated by

$$\frac{\mathrm{d}N^{\mathrm{cl}}}{\mathrm{d}E}\, 2\Delta E \approx 2(E/\hbar)^{3/2}\,, \tag{17}$$

where N^{cl} is the density of states (see (6), i.e. the surface of the three dimensional energy shell in phase space divided by $\hbar^{3/2}$. For $\hbar = 0.25$, this leads to approximately 10^3 states localizing on the energy shell $E = 20$.

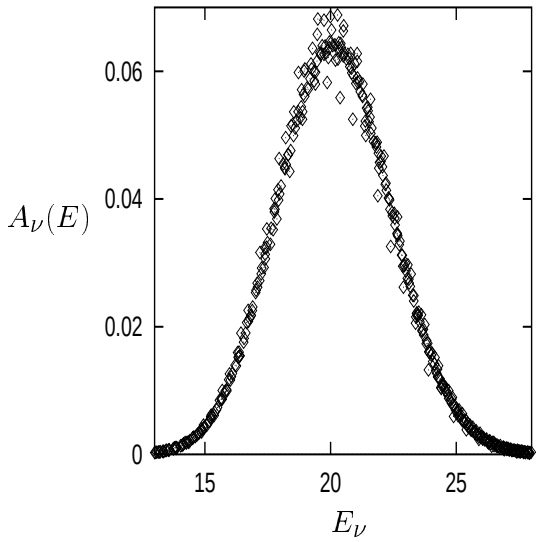

Figure 4. The density on the energy shell $A_\nu(E)$ as a function of the eigenenergy E_ν for a Poincaré section energy $E = 20$ for $\alpha = 0.1$, $\hbar = 0.25$. Shown are states of symmetry class $\mathcal{A}_1$.

2.3. Phase space localization

In Sect. 2.1 we have demonstrated that individual eigenstates $|\psi_\nu\rangle$ localize on different classical structures in phase space. A quantitative measure of the degree of (de)localization is provided by the Wehrl entropy [18, 19, 2]

$$S_\nu = -\int \frac{\mathrm{d}\vec{p}\,\mathrm{d}\vec{q}}{(2\pi\hbar)^2}\, \rho^{\mathrm{H}}_\nu(\vec{p},\vec{q}\,) \ln \rho^{\mathrm{H}}_\nu(\vec{p},\vec{q}\,)\,, \tag{18}$$

which satisfies the inequality $S_\nu \geq 2\,(=$ number of degrees of freedom). States, which are strongly localized in phase space, are expected to have a small entropy, as, e.g., the coherent states $|\vec{\alpha}\rangle$, whose entropy is equal to two.

The integration in (18) extends over the full four dimensional space, which is numerically very time consuming. In order to limit the numerical expense we therefore

restrict ourself in the present study to measure the quantum (de)localization on the Poincaré section, i.e. we restrict the integration over the two-dimensional surface of section (3):

$$S_\nu = -\int\limits_{\rm PSOS} \frac{{\rm d}p_x {\rm d}q_x}{2\pi\hbar}\, \tilde{\rho}_\nu^{\rm H}(p_x,q_x) \ln \tilde{\rho}_\nu^{\rm H}(p_x,q_x)\,, \tag{19}$$

where $\tilde{\rho}^{\rm H}$ is the renormalized Husimi density, i.e. $\rho_\nu^{\rm H}$ divided over its integral over the surface of section $A_\nu(E)$ (compare (11)). In addition, we take a Poincaré section at the dominant energy $E \approx E_\nu$ as discussed in Sect. 2.2.

Note that instead of the entropy (18) one can alternatively consider the integral over the square of the Husimi distribution

$$\xi_\nu^{-1} = \int\limits_{p_y^2 \le 2E} \frac{{\rm d}p_x {\rm d}q_x}{2\pi\hbar}\, \left[\tilde{\rho}_\nu^{\rm H}(p_x,q_x)\right]^2\,, \tag{20}$$

i.e. the 'mean inverse participation ratio', which is equivalent to the use of a different type of (Reny) entropy $S_\nu^{(2)} = \ln \xi_\nu$ instead of the Shannon-type entropy in (18) [4]. The results are similar.

An upper bound for the entropy (19) is given by a uniform density distribution over the classical Poincaré section, which gives

$$S_\nu^{\rm max} = \ln(E_\nu/\hbar) \tag{21}$$

i.e. $S_\nu^{\rm max} = 4.38$ for $E = 20$ ($\hbar = 0.25$) and $S_\nu^{\rm max} = 4.61$ for $E = 25$. A refined estimate of the maximum value can be obtained by assuming a uniform distribution over the classically chaotic region in phase space. A numerical computation of the classically chaotic phase space area yields for $\alpha = 0.05$ the values $S^{\rm max'} \approx 3.5$ ($E = 20$) and $S^{\rm max'} \approx 4.2$ ($E = 25$) For $\alpha = 0.1$ these values increase to 4.2 ($E = 20$) and 4.5 ($E = 25$).

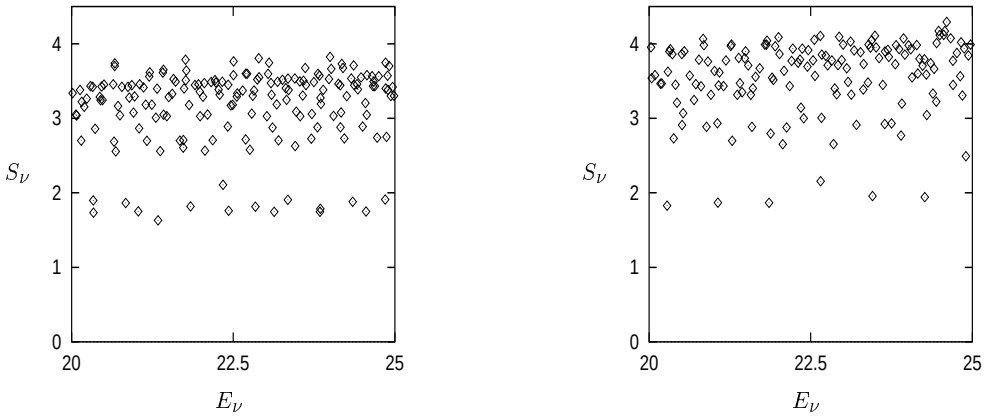

Figure 5. Phase space entropy $S^{(\nu)}$ versus the eigenenergy E_ν for eigenstates of the Pullen–Edmonds system ($\alpha = 0.1$, $\hbar = 0.25$) in the energy interval $20 \le E_\nu \le 25$.

Figure 5 shows the phase space entropy $S^{(\nu)}$ as a function of the eigenenergy E_ν for the eigenstates in the energy interval $20 \le E_\nu \le 25$ for $\alpha = 0.05$ and $\alpha = 0.1$, ($\hbar = 0.25$)

in the energy interval $20 \leq E_\nu \leq 25$. We observe a small fraction of strongly localized states with entropies close to two and a large fraction of highly delocalized (chaotic) states with entropies somewhat below $S^{\max'}$. Inspection of the Husimi densities shows that the low entropy states localize on the regular islands, as, e.g. states similar to (8) and (9) in figure 2. With increasing α the number of these regular states is reduced. The states with larger entropy populate the chaotic region.

3. Global phase space localization

As demonstrated in the previous section, the quantum phase space distributions ρ_ν^{H} of the eigenstates reflect and respect the classical dynamical properties in phase space. However, these states clearly show individual properties and it is desirable to develop a measure for the *global* dynamical properties of the quantum system at a given energy E, which is supposed to be a related to *all* eigenstates, with emphasis on those states with $E_\nu \approx E$, i.e. those states in the energy window given by ΔE_ν (compare Sect. 2.2).

Following [1, 4], the time evolved Husimi distribution of a wave packet $|\vec{\alpha}(t)\rangle$ initially centred at a phase space point $|\vec{\alpha}(0)\rangle = |\vec{\alpha}_0\rangle = |\vec{p}_0, \vec{q}_0\rangle$ is averaged over time:

$$\begin{aligned}
\bar{\rho}^{\mathrm{H}}(\vec{\alpha}, \vec{\alpha}_0) = \bar{\rho}^{\mathrm{H}}(\vec{p}, \vec{q}, \vec{p}_0, \vec{q}_0) &= \lim_{T\to\infty} \left(\frac{1}{T} \int_0^T \mathrm{d}t \; \rho^{\mathrm{H}}(\vec{\alpha}, \vec{\alpha}_0, t) \right) \\
&= \lim_{T\to\infty} \left(\frac{1}{T} \int_0^T \mathrm{d}t \; |\langle \vec{\alpha} | \vec{\alpha}_0(t) \rangle|^2 \right) \\
&= \lim_{T\to\infty} \left(\frac{1}{T} \int_0^T \mathrm{d}t \; \left| \langle \vec{\alpha}| \; \exp(-\frac{\mathrm{i}}{\hbar}\hat{H}t) \; |\vec{\alpha}_0\rangle \right|^2 \right) . \qquad (22)
\end{aligned}$$

This time averaged density describes the spreading of the initial wave packet over phase space. This delocalization can be quantitatively measured by the entropy

$$S(\vec{p}_0, \vec{q}_0) = -\int \frac{\mathrm{d}\vec{p}\,\mathrm{d}\vec{q}}{(2\pi\hbar)^2} \; \bar{\rho}^{\mathrm{H}}(\vec{p}, \vec{q}, \vec{p}_0, \vec{q}_0) \ln \bar{\rho}^{\mathrm{H}}(\vec{p}, \vec{q}, \vec{p}_0, \vec{q}_0) \, , \qquad (23)$$

or – when we again restrict the integration to the two-dimensional surface of section (3) – by

$$\begin{aligned}
S(p_{x_0}, q_{x_0}) &= -\int_{\mathrm{PSOS}} \frac{\mathrm{d}p_x \mathrm{d}q_x}{2\pi\hbar} \; \widetilde{\rho}^{\mathrm{H}} \ln \widetilde{\rho}^{\mathrm{H}} \\
&= -\int_{p_y^2 \leq 2E} \frac{\mathrm{d}p_x \mathrm{d}q_x}{2\pi\hbar} \; \widetilde{\rho}^{\mathrm{H}}(p_x, q_x, p_{x_0}, q_{x_0}) \ln \widetilde{\rho}^{\mathrm{H}}(p_x, q_x, p_{x_0}, q_{x_0}), \qquad (24)
\end{aligned}$$

where $\widetilde{\rho}^{\mathrm{H}}$ is the renormalized time averaged Husimi density, i.e. $\bar{\rho}^{\mathrm{H}}$ divided over its integral over the surface of section. In order to compare with the classical Poincaré section, it is natural to vary the initial conditions $(\vec{p}_0, \vec{q}_0)$ over the two-dimensional classical surface of section. A plot of $S(p_{x_0}, q_{x_0})$ shows the overall delocalization over the Poincaré section for a coherent wavepacket initially placed at (p_{x_0}, q_{x_0}) Similar concepts

have been suggested by Thiele and coworkers [20, 21] and by Müller [22] (see also the early papers by Nordholm and Rice [23, 24]); for a general discussion of the use and properties of entropies for analysing quantum localization see [4] and references therein.

The numerical computation is very much simplified by means of a decomposition in eigenstates

$$\begin{aligned}\bar{\rho}^{\mathrm{H}}(\vec{\alpha},\vec{\alpha}_0) &= \lim_{T\to\infty}\frac{1}{T}\int_0^T \mathrm{d}t\ \left|\sum_\nu \mathrm{e}^{-\frac{\mathrm{i}}{\hbar}E_\nu t}\ \langle\vec{\alpha}|\psi_\nu\rangle\langle\psi_\nu|\vec{\alpha}_0\rangle\right|^2 \\ &= \lim_{T\to\infty}\frac{1}{T}\int_0^T \mathrm{d}t\ \sum_\nu |\langle\vec{\alpha}|\psi_\nu\rangle|^2\ |\langle\vec{\alpha}_0|\psi_\nu\rangle|^2 \qquad (25)\\ &+\sum_{\mu\neq\nu}\mathrm{e}^{-\frac{\mathrm{i}}{\hbar}(E_\nu-E_\mu)\,t}\ \langle\vec{\alpha}|\psi_\nu\rangle\langle\psi_\nu|\vec{\alpha}_0\rangle\langle\vec{\alpha}_0|\psi_\mu\rangle\rangle\langle\psi_\mu|\vec{\alpha}\rangle = \sum_\nu |\langle\vec{\alpha}|\psi_\nu\rangle|^2\ |\langle\vec{\alpha}_0|\psi_\nu\rangle|^2\,,\end{aligned}$$

where the last equality assumes non-degenerate states, i.e. it is not valid for the states in class $\mathcal{H}_{\mathcal{E}}$. In the following we only consider the non-degenerate states of classes $\mathcal{H}_{\mathcal{A}_1}, \mathcal{H}_{\mathcal{A}_2}, \mathcal{H}_{\mathcal{B}_1}, \mathcal{H}_{\mathcal{B}_2}$, i.e., we use initial states in (22), which are coherent states $|\vec{\alpha}_0\rangle$ projected onto the union of these subspaces. which yields

$$\bar{\rho}^{\mathrm{H}}_{\mathrm{sym}}(\vec{\alpha},\vec{\alpha}_0) = \sum_{\nu'} |\langle\vec{\alpha}|\psi_{\nu'}\rangle|^2\ |\langle\vec{\alpha}_0|\psi_{\nu'}\rangle|^2 \qquad (26)$$

where the sum includes all $|\psi_\nu\rangle \in \{\mathcal{H}_{\mathcal{A}_1}, \mathcal{H}_{\mathcal{A}_2}, \mathcal{H}_{\mathcal{B}_1}, \mathcal{H}_{\mathcal{B}_2}\}$.

In the numerical computation, the infinite sum in (26) can be truncated in view of the localization on the energy shell (see Sect. 2.2). For $E = 20$, for example, only states

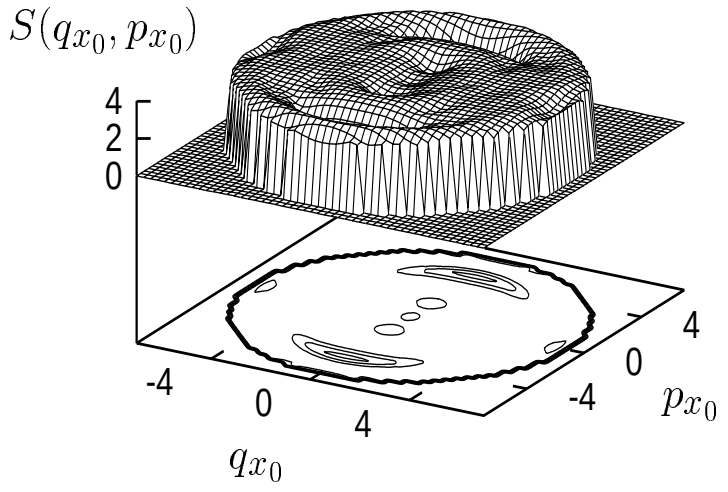

Figure 6. Global quantum phase space entropy $S(p_{x_0}, q_{x_0})$ of the Pullen–Edmonds system ($\alpha = 0.05$, $\hbar = 0.25$) for $E = 20$ as a contour plot over phase space.

in the interval $15 < E_\nu < 25$ considerably contribute.

Figure 6 shows the global quantum phase space entropy $S(p_{x_0}, q_{x_0})$ for the Pullen–Edmonds system ($\alpha = 0.05$, $\hbar = 0.25$) for $E = 20$ as a contour plot over phase space. A comparison with figure 1 shows a clear correspondence between quantum and classical phase space structures. The big resonance islands are clearly visible, however the satellite islands are not resolved for $\hbar = 0.25$. An additional quantum localization on the unstable hyperbolic fixed point at $(p_x, q_x) \approx (0, \pm 4)$ appears as a local minimum of the entropy. Figure 7 shows the same plot, however for an increased value of the nonlinearity parameter $\alpha = 0.1$. Also here we find a remarkable agreement with the classical Poincaré section, i.e. the four outer islands and the bifurcated central resonance, appearing as two small resonances. Again we observe a strong quantum localization at the classically unstable fixed point at the centre.

Horizontal and vertical cuts through the entropy plots in Figs. 6 and 7 are shown in Figs. 8 and 9, respectively. For $\alpha = 0.05$ the entropy is clearly smaller than the upper estimate of $S^{\max} = 4.38$ (uniform density over the Poincaré section as discussed in Sect. 2.3), however it considerably exceeds the estimate $S^{\max'} \approx 3.5$ (uniform distribution on the classically chaotic region). This can be attributed to the marked population of the Husimi distributions of the chaotic quantum states in the regular regions. Similarly for $\alpha = 0.1$, where the estimate $S^{\max'} \approx 4.2$ is slightly exceeded. At the centres of the big stability islands, the entropy shows deep minima, where its value is approximately equal to two, which is the global minimum of the Wehrl entropy

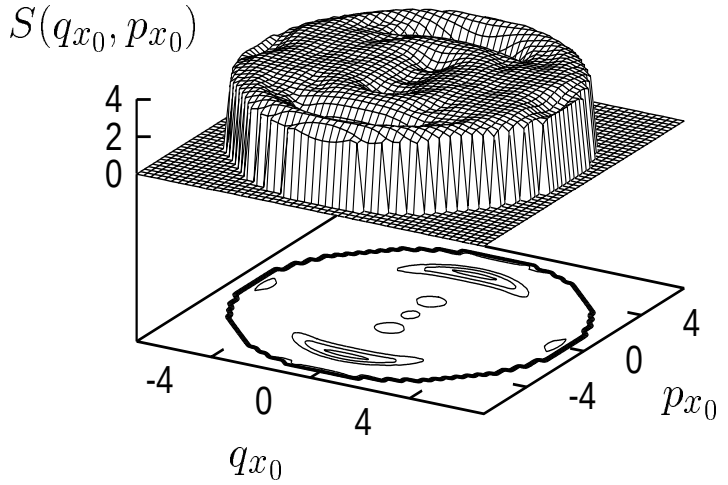

Figure 7. Same as figure 6, however for an increased value of the nonlinearity parameter $\alpha = 0.1$.

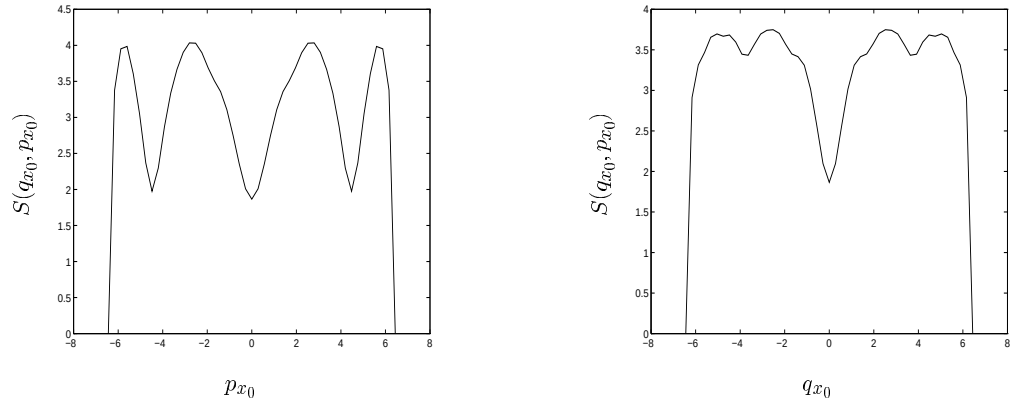

Figure 8. Global quantum phase space entropy $S(p_{x_0}, q_{x_0})$ the Pullen–Edmonds system ($\alpha = 0.05$, $\hbar = 0.25$) as a function of q_{x_0} for $p_{x_0} = 0$ (left) and p_{x_0} for $q_{x_0} = 0$ (right).

(18) or (19), i.e. the Husimi density is close to a coherent state in these points. The localization at the other stable or unstable fixed points is much less pronounced.

4. Conclusions

In this paper we have extended the concept of quantum phase space entropies, which has previously been developed in studies of one-dimensional systems, to the case of two degrees of freedom. We have demonstrated that the method provides a convenient diagnostic tool for analysing and visualising the dynamical properties of quantum systems in phase space. The resulting entropy plots are in close relationship to the Poincaré surfaces of section in the study of classical dynamics. Moreover, it has been

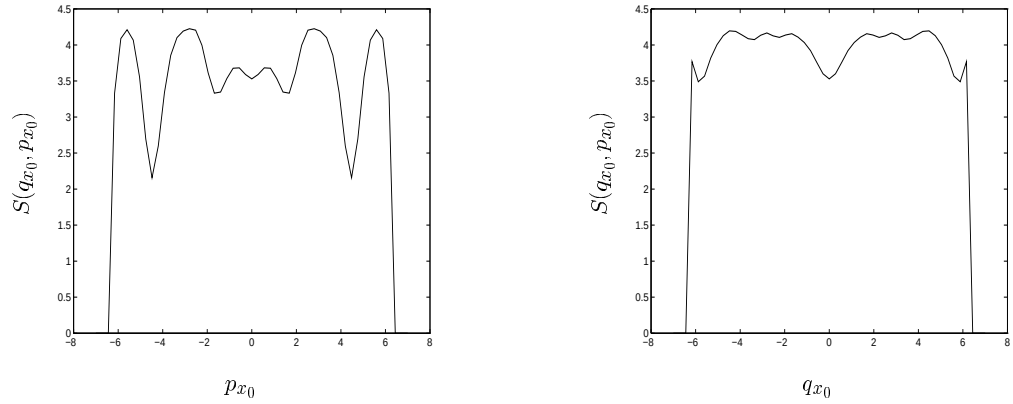

Figure 9. Global quantum phase space entropy $S(p_{x_0}, q_{x_0})$ the Pullen–Edmonds system ($\alpha = 0.1$, $\hbar = 0.25$) as a function of q_{x_0} for $p_{x_0} = 0$ (left) and p_{x_0} for $q_{x_0} = 0$ (right).

pointed out [1, 4] that the concept of a quantum entropy has a direct counterpart in classical mechanics, which offers the possibility of a direct comparison of classical and quantum properties to detect, e.g., quantum localization phenomena. This question has not been addressed in the present study. Clearly, much more work is required to explore the properties of the phase space entropy concept, both in quantum and classical dynamics.

Acknowledgments

This work has been supported by the Deutsche Forschungsgemeinschaft (SPP *'Zeitabhängige Phänomene und Methoden in Quantensystemen der Physik und Chemie'*).

References

[1] Mirbach B and Korsch H J 1995 Phys. Rev. Lett. **75** 362
[2] Gorin T, Korsch H J and B Mirbach 1997 Chem. Phys. **217** 145
[3] Wiescher H and Korsch H J 1997 J. Phys. A **30** 1763
[4] Mirbach B and Korsch H J 1998 Ann. Phys., NY in press
[5] Pullen R A and Edmonds A R 1981 J. Phys. A **14** L477
[6] Feingold M, Moiseyev N and Peres A 1985 Chem. Phys. Lett. **117** 344
[7] Meyer H D J. Chem. Phys. 1986 **84** 3147
[8] R L Waterland R L, Yuan J-M, Martens C C, Gillilan R E and Reinhardt W P 1988 Phys. Rev. Lett. **24** 2933
[9] Anchell J A 1990 J. Chem. Phys. **92** 4342
[10] Zeng Y H and Serota R A 1994 Phys. Rev. B **50** 2492
[11] Ericson T and Ruhe A 1980 Mathematics of Computation **35** 1251
[12] Groh G 1997 Diplomarbeit University Kaiserslautern
[13] Weissman Y and Jortner J 1982 J. Chem. Phys. **77** 1486
[14] Leboeuf P and Voros A 1990 J. Phys. A **23** 1765
[15] Dando P A and Monteiro T S 1994 J. Phys. B **27** 2681
[16] Müller K and Wintgen D 1994 J. Phys. B **27** 2693
[17] Arranz F J, Borondo F and Benito R M 1996 Phys. Rev. E **54** () 2458
[18] Wehrl A 1978 Rev. Mod. Phys. **50** 221
[19] Orlowski A 1993 Phys. Rev. A **48** 727
[20] Thiele E and Stone J 1984 J. Chem. Phys. **80** 5187
[21] Thiele E, Stone J and Goodman M F 1982 in *Intramolecular Dynamics* ed J Jortner and B Pullman (Reidel Publishing Company) p 391
[22] Müller K 1992 Thesis University Heidelberg
[23] Nordholm K S J and Rice S A 1974 J. Chem. Phys. **61** 203
[24] Nordholm S and Rice S A 1974 J. Chem. Phys. **61** 768